Colloid Polym Sci 277:361–371 (1999)

ORIGINAL CONTRIBUTION

N. Hattori
H. Hirata
H. Okabayashi
C.J. O'Connor

Small-angle neutron-scattering study and micellar model of the gemini (phenylene-dimethylene)bis(*n*-octylammonium)dibromide surfactant micelles in water

Received: 8 September 1998
Accepted in revised form: 27 November 1998

N. Hattori · H. Hirata
H. Okabayashi (✉)
Department of Applied Chemistry
Nagoya Institute of Technology
Gokiso-cho, Showa-ku
Nagoya 466-8555, Japan
Fax: +81-52-735+5247

C.J. O'Connor
Department of Chemistry
The University of Auckland
PB 92019, Auckland
New Zealand

Abstract The microstructure of the micelles formed in aqueous solution by gemini surfactants with aromatic spacers, $[Br(CH_3)_2N^+(C_mH_{2m+1})$-(Ph)-$(C_mH_{2m+1})N^+(CH_3)_2Br$, $m = 8$ and Ph = *o*-, *m*- or *p*-phenylene-dimethylene] has been examined by small-angle neutron scattering. Aggregation of the gemini surfactants with an *o*-phenylenedimethylene spacer brings about formation of premicelles and small micelles at concentrations below the second critical micelle concentration, while above this concentration marked micellar growth and variation in shape occurs. It is suggested that the minimum aggregate formed at this critical micelle concentration may be the trimer or tetramer and that this result supports the mechanism of "gemini → submicelle → assembly" for micellar growth.

Key words Gemini surfactant – Small-Angle Neutron-Scattering – Micellar model

Introduction

Menger and Littau [1] assigned the name "gemini surfactants" to dimeric surfactants with rigid spacers and considerable attention has been given to the behavior of their solutions and of their monolayers formed at an air/water interface [2–11]. In particular, some unusual behavior of the geminis has been noted. For example, Menger and Littau [2] reported that for the stilbene-based geminis with hydrocarbon chains of carbon number $n_c = 12$, 16 and 20, longer-chain geminis are associated with higher critical micelle concentration (cmc) values. It is most unusual that the value of the cmc should increase with an increase in chain length. Furthermore, they also suggested that longer-chain geminis engage in self-coiling or submicellar aggregation when first exposed to water [2]; however, the mechanism of self-assembly for gemini surfactants still remains obscure, although several hypotheses have been presented [3–5]. If one is to understand the details of this peculiar "non-classical" behavior for the geminis then it should be rationalized at a molecular level.

Recently, we have demonstrated that a conformational change occurs upon micellization of gemini surfactants in which two quaternary ammonium species $[CH_3(CH_2)_7N^+(CH_3)_2]$ are linked at the polar head groups by an *o*- and *m*-phenylenedimethylene spacer [12, 13]. The results showed that the specific rotational isomers about the CH_2-aromatic carbon single bonds for the gemini surfactant having a *m*-phenylene-dimethylene spacer are preferentially stabilized upon aggregation, while for the gemini having an *o*-phenylene-dimethylene spacer only the conformation in which the aromatic ring is sandwiched between two *n*-octyl chains is stabilized.

In the present study, the results of small-angle neutron-scattering (SANS) analysis have been used to discuss in detail the structure of the normal micelles formed by gemini surfactants with phenylenedimethlyene spacers, and this has assisted our further understanding of their unusual behavior at the molecular level.

Experimental

Materials

(Phenylenedimethylene)bis(*n*-octylammonium)dibromide surfactants (Fig. 1) were synthesized as follows. For oxy8, mxy8 and pxy8, reactions of *n*-octyldimethylamine with the corresponding *o*-, *m*-, or *p*-phenylenedimethylene dibromides, respectively, [14], were performed in dried ethanol under reflux ($T = 353$ K) for 24 h so as to ensure as complete bisquarternarization as possible. The three gemini surfactants thus synthesized were recrystallized in ethanol-ether or acetone-ether. Sample identification was confirmed by NMR and elemental analysis. The reactants, which were purchased from Tokyo Kasei Co., were purified before use.

Conductivity and ^{1}H NMR chemical-shift measurements and cmc determination

The electrical conductivity of the sample solution was measured with a CM-11P conductivity meter (TOA-Electronics) at 25.0 ± 0.1 °C. The cmc were determined from plots of specific electrical conductivity against surfactant concentration. The cmc (first cmc) values thus obtained were 1.36 wt% for oxy8, 1.31 wt% for mxy8 and 1.42 wt% for pxy8. For oxy8, the value of a second cmc (3.4 wt%) was also obtained. The values of the first and second cmcs for oxy8 were also determined from plots of the ^{1}H chemical shift (δ ppm) for aromatic protons versus concentration and are 2.0 and 3.7 wt%, respectively.

Neutron-scattering measurements

The SANS measurements were carried out using the medium-angle neutron-scattering instrument (WINK) installed at the pulsed neutron source KENS at the National Laboratory for High Energy Physics, Tsukuba, Japan. The sample solutions were placed in a quartz cell of 2 mm path length at 23 °C. The scattering length density (ρ) of each component was calculated using Eq. (1),

$$\rho = \Sigma b_i / V \quad , \tag{1}$$

where b_i is the scattering length of atom i and V is the molecular volume. The V values, calculated from partial molar volume data measured in the present study, and Σb_i values quoted from Ref. [15], are listed in Table 1. The magnitude of the momentum transfer (Q) is given by Eq. (2),

$$Q = \frac{4\pi}{\lambda} \sin\left(\frac{\theta}{2}\right) \quad , \tag{2}$$

where λ is the incident wavelength (1–16 Å for WINK). The intensity of scattered neutrons was recorded on a position- sensitive 2D detector. Normalization of the data to an absolute intensity scale was made by using the transmission of a 1 mm water sample. Corrections for the attenuation of the beam due to absorption and for multiple scattering were also made.

In the SANS analysis, the scattering intensity coming from the gemini surfactant solution was corrected for the detector background and incoherent scattering. The intensity spectrum of the sample solution measured at concentrations below the cmc was subtracted from those of the micellar solutions in the Q range 0.06–0.30 Å^{-1}.

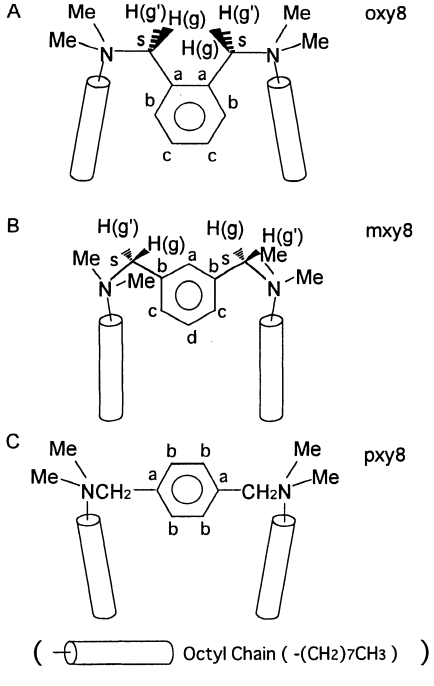

Fig. 1 Schematic molecular models of *oxy*8, *mxy*8 and *pxy*8

Table 1 Volumes (V) and scattering lengths (Σb_{coh})

Species	V [Å^3]	Σb_{coh} [Å]
CH_3	42.6	-0.457×10^{-4}
CH_2	28.2	-0.083×10^{-4}
Ph	110.6	2.493×10^{-4}
N^+	−30.5	0.936×10^{-4}
Br^-	50.0	0.677×10^{-4}
D_2O	30.3	1.918×10^{-4}

SANS analysis

The dependence of the neutron-scattering intensity $d\Sigma(Q)/d\Omega$ on the magnitude of a scattering vector (Q) can be expressed as a function of both the particle structure factor $P(Q)$ and the size- and orientation-weighted interparticle-structure factor $S'(Q)$, as follows,

$$d\Sigma(Q)/d\Omega = I_0 P(Q) S'(Q) \quad , \tag{3}$$

where I_0 is the extrapolated zero-angle scattering intensity, which is independent of the micellar shape. Furthermore, I_0 is a function of the average aggregation number n and is expressed by Eq. (4) in terms of the volumes of the micelle core (V_o, in Å^3) and overall micelle (V_m, in Å^3) and the average neutron-scattering length densities of the polar shell, hydrophobic core and solvent (ρ_p, ρ_c and ρ_s, in Å^2, respectively).

$$I_0 = \frac{(C - cmc)N_A}{1000n} 10^{-16} \left[(\rho_p - \rho_c) V_c + (\rho_s - \rho_p) V_m \right]^2 \quad , \tag{4}$$

where N_A is Avogadro's number. When the interaction between micelles is neglected, the interparticle structure factor is reduced to unity [$S'(Q) = 1$]. In the small-angle scattering region, the terms in Eq. (3) can be written in the Guinier approximation [16] in the following form.

$$\ln \frac{d\Sigma(Q)}{d\Omega} = \ln I_0 - \frac{R_g^2}{3} Q^2 \quad , \tag{5}$$

where R_g is the radius of gyration of the particle.

The particle structure factor $P(Q)$ for an ellipsoid particle is given by Eq. (6),

$$P(Q) = \int_0^1 |F(Q,\mu)|^2 \, d\mu \quad , \tag{6}$$

where

$$F(Q,\mu) = x\left(\frac{3[\sin(QR_1) - QR_1\cos(QR_1)]}{(QR_1)^3}\right) + (1-x)\left(\frac{3[\sin(QR_2) - QR_2\cos(QR_2)]}{(QR_2)^3}\right) \tag{7}$$

$$x = (\rho_p - \rho_c)V_c / [(\rho_p - \rho_c)V_c + (\rho_s - \rho_p)V_m] \quad . \tag{8}$$

R_1 and R_2 are given by

$$R_1 = [a^2\mu^2 + b^2(1-\mu^2)]^{1/2} \tag{9}$$

$$R_2 = [(a+t)^2\mu^2 + (b+t)^2(1-\mu)^2]^{1/2} \tag{10}$$

for the prolate model where a and b are the major and minor axes of a micellar particle, t is the thickness of the polar core of a micellar particle, and μ is the cosine of the angle between the direction of the minor axis b and the scattering vector Q.

For micellar solution systems having interparticle electrostatic interactions, the interaction peak appears in the SANS intensity spectrum. Therefore, in order to explain the observed SANS spectrum, it is necessary to calculate I_0 and $S'(Q)$, in addition to $P(Q)$, on the basis of a micellar model.

In order to take into account the electrostatic interactions between charged aggregate particles, the mean spherical approximation (MSA) method was originally proposed by Lebowitz and Percus [17], and was solved by Waisman and Lebowitz [18] for the system containing equally sized particles of opposite charge, and by Blum and Hoye [19] for the general case of arbitrary charge and size. Triolo and Floriano [20] have provided structural functions for ionic systems by use of this method.

The MSA model has also been solved by Hayter [21] and by Baus and Hansen [22] for a one-component macrofluid and by Palmer and Weeks [23] who again treated a system of charged hard spheres with an unscreened Coulombic potential as a one-component macrofluid. A numerical solution for the system of charged particles interacting through a screened Coulombic potential has been provided by Waisman [24].

Hayter and Penfold [25, 26] demonstrated that the SANS spectra coming from a micellar solution could be well described by treating the solution as a one-component macrofluid. Furthermore, Hansen and Hayter [27] provided a means (the rescaling procedure, so-called RMSA) of calculating an interparticle structure factor [$S'(Q)$] for a one-component macrofluid.

The size- and orientation-weighted interparticle structure factor $S'(Q)$ can be calculated [27, 28] by use of Eq. (11),

$$S'(Q) = 1 + \beta(Q,\mu)[S(Q) - 1] \quad , \tag{11}$$

where

$$\beta(Q,\mu) = \left|\langle F(Q,\mu)\rangle^2\right| / \left\langle |F(Q,\mu)|^2 \right\rangle \quad . \tag{12}$$

When the micellar model for $P(Q)$ translates into the model for $S(Q)$, the micelle is assumed to be a rigid charged sphere of diameter σ, interacting through a dimensionless screened Coulombic potential, which is calculated by using the inverse screening length of Debye–Hückel theory, defined by the ionic strength, I, of the solution. This assumption is reasonable for charged micelles if the a/b ratio is not much greater than unity. Furthermore, it has been shown that one may approximate the micellar core as a rigid sphere, provided that the shape of the ionic micelle is ellipsoidal with an a/b ratio no greater than 2 [28]. For systems with an a/b ratio greater than 2, Kotlarchyk and Chen [28] have proposed another approach with a more accurate prescription of the diameter σ, in which orientational averaging of particles affects $S'(Q)$. This procedure has been successfully used to interpret the SANS spectra of the native protein, bovine serum albumin, in the monodispersed state [28].

In this present study, for analysis of the SANS spectra of the oxy8 sample solutions, in which the peak arising from the intermicellar interactions disappears, Eq. (3), which assumes that $S'(Q)$ is equal to unity, was used. In the analysis of those SANS spectra which had an interaction peak, the macroion diameter σ, which has been more accurately prescribed [28], and which is given by Eq. (13), was used for the calculation of $S'(Q)$.

$$\sigma = \left[2(f+1)(a+t)(b+t)^2\right]^{1/3} \quad , \tag{13}$$

where

$$f = \frac{3}{4}\left(1 + \frac{\sin^{-1} P}{P(1-P^2)^{1/2}}\right)\left[1 + \frac{1-P^2}{2P}\ln\left(\frac{1+P}{1-P}\right)\right] \tag{14}$$

$$P = \left[\frac{(a+t)^2 - (b+t)^2}{(a+t)^2}\right]^{1/2} \quad . \tag{15}$$

For the size-dispersed system of charged hard particles, the scattering intensity can be expressed in the following form,

$$\frac{d\Sigma(Q)}{d\Omega} = \left(\sum_{i=i_{min}}^{i_{max}} n_p(i)\left\{[\rho_p(i) - \rho_c(i)]V_c(i) + [\rho_s(i) - \rho_p(i)]V_m(i)\right\}^2 P(i,Q)\right) S'(Q) \tag{16}$$

$$n_p(i) = \frac{(C - cmc)d(i)N_A}{1000i} \ [cm^{-3}] \quad , \tag{17}$$

where (i) denotes the particles having aggregation number i, and $d(i)$ is the concentration distribution function of the monomer. In this present study, it was assumed that $d(i)$ is a Gaussian function with a standard deviation (square root of mean average aggregation number) [29].

Results and discussion

Conformational basis for the micellar model

We have reported selective-decoupling ^{13}C NMR spectroscopic evidence for the conformational change of the cations of the gemini surfactants oxy8 and mxy8 upon micellization in water [12]. Results of special relevance to this study may be summarized as follows.

For oxy8, it was found that the original gg′ form about the $^{s}CH_2$—^{a}C single bond is stabilized in both the monomeric and micellar states and that the two *n*-octyl-N segments are in a trans configuration with respect to the ^{a}C—^{a}C bond (Fig. 1).

For an mxy8 molecule in solution, six skeletal structures are expected, since three rotational isomers [(trans (t), gauche (g) and gauche′ (g′)] about the $^{s}CH_2$—^{b}C single bond are possible, as listed in Table 2. When the ^{b}C—^{a}C bond is regarded as a criterion for the t, g and g′ configurations, types I, II and III are possible.

Table 2 Possible skeletal structures of an mxy8 molecule

Criterion: ^{b}C—^{a}C		Criterion: ^{b}C—^{c}C	
Type I	gg′gg′	Type I′	tgtg(tg′tg′) tg′tg(tgtg′)
Type II	tggg′(tg′gg′)	Type II′	tggg′(tg′gg′)
Type III	tgtg (tg′tg′) tg′tg (tgtg′)	Type III′	gg′gg′

When we take the ^{b}C—^{c}C bond as a criterion for the three configurations, types I′, II′ and III′ are possible. We have found by use of a selective-decoupling ^{13}C NMR technique that micellization brings about preferential stabilization of the type I structure (Fig. 1), in which both of the $N^{s}C^{b}C$-planes are coplanar with the benzene plane and in the Newman projection the two *n*-octyl-N segments are in the trans configuration with respect to the ^{a}C—^{b}C bond. Furthermore, in a previous paper [13], it was reported that for oxy8 and mxy8 variation in the stacking pattern of the aromatic rings after micellization of these surfactants is markedly reflected in the ^{1}H spectral features of the aromatic protons. This result provides evidence that the stacking feature of the aromatic rings in the oxy8 micelles changes below and above the first cmc (2.0 wt%) or the second cmc (3.7 wt%), which were determined by the ^{1}H NMR method [13], and that there exists a relationship between the variation in the stacking manner and the preferential stabilization of a specific rotational isomer.

Thus, preferential stabilization of a specific isomer reveals that the N—^{s}C—^{a}C—^{a}C—^{s}C—N (oxy8) and N—^{s}C—^{b}C—^{a}C—^{b}C—^{s}C—N (mxy8) skeletons containing the benzene ring are rigid and planar. This fact is important in discussing the orientation of the gemini molecules in micelles, since the rigidity and planarity of such a skeleton play a significant role in the micellar orientation of the molecules, which affects the shape and size of the micelles.

The specific molecular conformation of the N—^{s}C—^{b}C—^{a}C—^{b}C—^{s}C—N skeleton for mxy8, which is stabilized upon micellization, and that for the N—^{s}C—^{a}C—^{a}C—^{s}C—N skeleton of oxy8, which is stabilized in both its monomeric and micellar states, were used to discuss the micellar structure of the geminis.

Conformational studies on the hydrocarbon portion of surfactants in the aggregated state are important for understanding the aggregated structure. Thus far, for potassium *n*-butanoate [$CH_3(CH_2)_2COOK$], *n*-pentanoate [$CH_3(CH_2)_3COOK$] and *n*-hexanoate [$CH_3(CH_2)_4COOK$] in the solid state and in aqueous solution, Raman-scattering spectra have also been measured, and the concentration dependence of the molecular conformations for these molecules has been investigated in detail by use of the accordion vibrations characteristic of the fully extended hydrocarbon chains [30]. The results

have indicated that the percentage of the fully extended form increases with an increase in concentration above the cmc.

Furthermore, detailed conformational analysis has been carried out for potassium *n*-pentanoate and *n*-hexanoate by use of the normal coordinate analysis for the possible rotational isomers [31], revealing that for the *n*-pentanoate anion the TT form is more stable than the GT and TG forms in the micellar state and that for the *n*-hexanoate anion the TTT form is more stable than are the other three isomers (TGT, GTT and TGG).

For the longer *n*-octanoate and *n*-decanoate anions in aqueous solution, the accordion bands arising from the all-trans forms were not observed in dilute micellar solutions, although they were found only in concentrated solutions. In particular, it should be emphasized that the other isomers containing one gauche form (e.g. GTTTT or TGTTT forms for $CH_3CH_2CH_2CH_2CH_2CH_2CH_2COOK$) may be relatively stable, if evidence from the Raman spectra of *n*-paraffins [32] and soap molecules [31] is used as an analogy.

Recently, we have also reported the Raman-scattering study of tetra-, hexa-, octa- and deca-methonium bromides $[Br^-(CH_3)_3N^+—(CH_2)_n—N^+(CH_3)_3Br^-$, $n = 4$, 6, 8 and 10] in the solid state and in aqueous solution [33]. The results show that a fully extended conformation, similar to that which exists in the solid state, is stabilized in aqueous solution and especially in more concentrated solutions.

From these experimental result, it may be assumed that fully extended shorter polymethylene segments [$(CH_2)_n$, $n = 2$–6] are relatively stabilized and that their populations are very high. Therefore, one may assume that in longer polymethylene chains some shorter extended segments are folded by gauche bond rotations: for example, the octyl chains ($^1CH_2—^2CH_2—^3CH_2—^4CH_2—^5CH_2—^6CH_2—^7CH_2—^8CH_3$) of the present gemini surfactants may be made up of a combination of the extended $^1CH_2 \cdots ^6CH_2$ segment and the gauche form of the $^6CH_2—^7CH_2$ segment. This assumption can be used to make up a micellar model for an oxy8-D_2O system.

Micellar models for oxy8

In general, a surfactant molecule with a planar structure tends to form a disk or cylindrical aggregate [28]. However, an oxy8 molecule has one planar aromatic ring and two flexible octyl chains; therefore, we may expect that flexible octyl chains play an important role in the aggregate structure [12], leading to the formation of other types of aggregates.

Thus, we may assume that for the *n*-octyl chain of an oxy8 molecule, in addition to preferential stabilization of the extended form upon micellization, further increase in the population of the all-trans form occurs above the second cmc (3.7 wt%), and that the fraction of the extended form increases more above the second cmc. This assumption, which is based on experimental evidence, is important in establishing the micellar model.

An outline of the structural model of an oxy8 micelle, which was used in the calculation of the single particle form factor $P(Q)$, is shown in Fig. 2 only for the prolate model, since this model provided a better fit than did the oblate model, particularly for concentrated sample solutions.

The shape of an oxy8 micelle is prolate spheroidal and has a hydrophobic core with a major axis a and minor axis b. The value of a is expressed by Eq. (18),

$$a = (3V_{\text{tail}}/(4\pi n b^2)[\text{Å}] \ , \tag{18}$$

where V_{tail} is the volume of the hydrophobic portions and n is the aggregation number. The b value is given by Eq. (19) [34],

$$b = \rho(1.5 + 1.265(8 - n_{\text{wet}}))[\text{Å}] \ , \tag{19}$$

where ρ is the ratio of a flexible to a fully extended chain and n_{wet} is the number of hydrated methylenes of an *n*-octyl chain.

Since there exists a marked difference in the SANS intensity spectra of oxy8 below and above the second cmc, we may expect that formation of smaller oxy8 micelles occurs below the second cmc and that the larger micelles are formed upon secondary aggregation above the cmc. Thus, in the present study, on the basis of previous experimental data, we propose two kinds of micellar models for small and large oxy8 micellar systems. We assume that the *n*-octyl chains ($CH_3CH_2CH_2CH_2CH_2CH_2CH_2CH_2—$) take the GTTTTT form for the small micelle system and the all-trans forms for the large micelle system. In the structural model of an oxy8 micelle (Fig. 2A), it was assumed that the ρ value of the octyl chain is equal to 0.8 for smaller micelles and to 1.0 for larger micelles.

The hydrophilic layer, of thickness t, consists of head groups including the $^+N(CH_3)_2$ groups, associated with bromide anions and water molecules, the hydrated methylene groups of the *n*-octyl chain and the hydrated portion of a benzene ring and has a value given by Eq. (20).

$$t = \rho[1.5 + 1.265(2 + n_{\text{wet}})]\,[\text{Å}] \ . \tag{20}$$

The volume of the hydrophobic portions constituting the core (V_{tail}) and that of the polar heads in the hydrophilic layer (V_{head}), which were used for calculation of the scattering length densities of the whole micelle, are expressed by Eqs. (21) and (22),

$$V_{\text{tail}} = 2[V_{CH_3} + (9 - n_{\text{wet}})V_{CH_2}] + V_{\text{ph}} \tag{21}$$

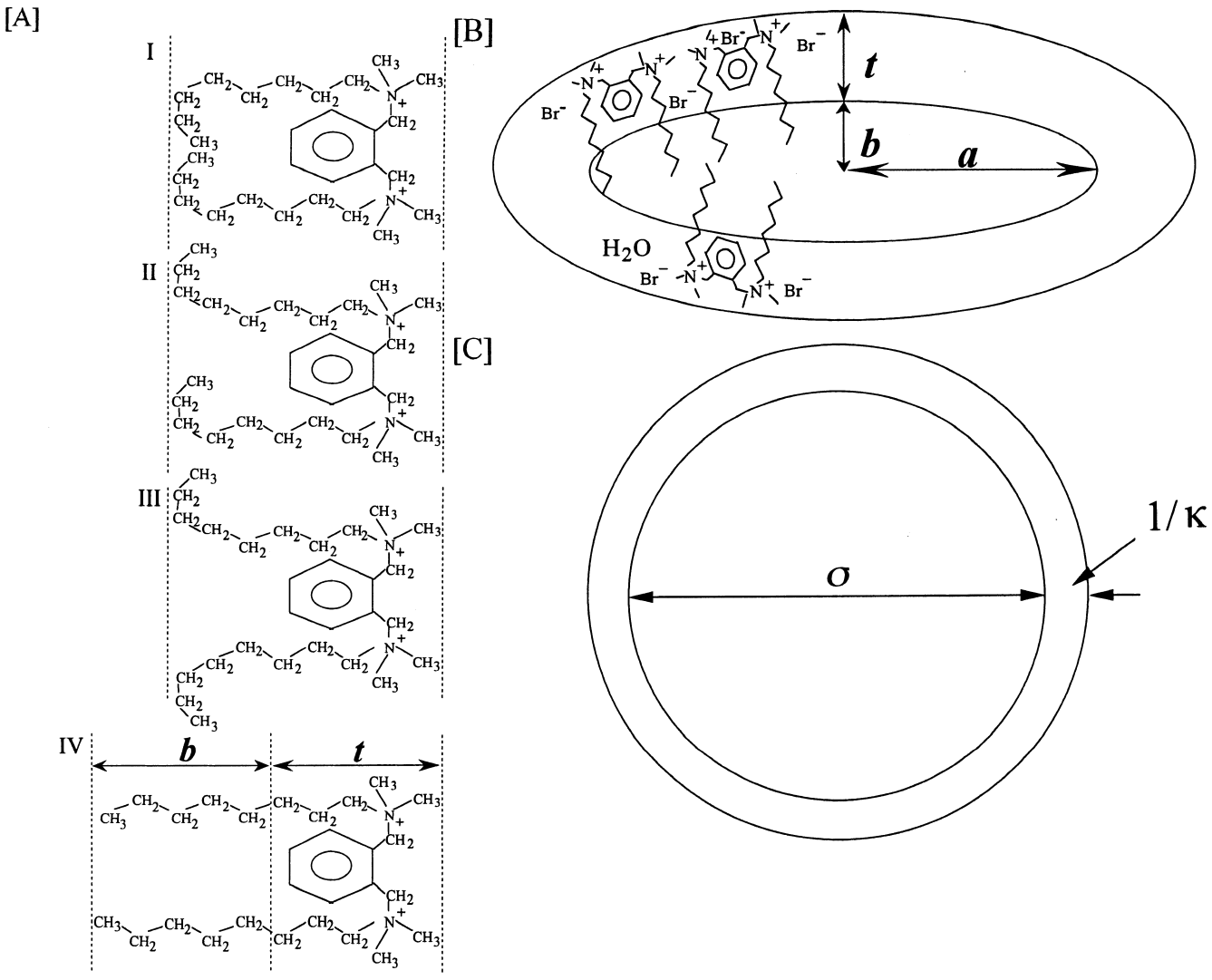

Fig. 2 **A** Suggested molecular model (*I*, *II* and *III* for a small micelle and *IV* for a long micelle) for oxy8. In the micellar models used in the calculation of **B** $P(Q)$ and **C** $S'(Q)$, t is the thickness of the Stern layer, a and b are the major and minor axes, respectively, σ is the diameter of a macroion and $1/\kappa$ is the inverse Debye–Hückel screening length

$$V_{\text{head}} = 2(2V_{\text{CH}_3} + n_{\text{wet}}V_{\text{CH}_2} + V_{\text{N}}) + 2V_{\text{CH}_2} + V_{\text{ph}} \quad , \qquad (22)$$

where V_{CH_3}, V_{CH_2}, V_{ph} and V_{N} are the volumes of the methyl, methylene, phenyl groups and of the nitrogen atom, respectively. These values were calculated using partial molar volume data listed in Table 1.

SANS spectra and micellar growth

In this present study, the SANS spectra of oxy8, mxy8 and pxy8 in D_2O have been measured. For the micelles formed by the oxy8 molecules, calculations have been made for both prolate and oblate spheroidal models by assuming monodispersity.

In the curves of $I(Q)$ against Q observed at concentrations less than 3.0 wt% (Fig. 3), the peaks arising from the intermicellar interactions disappear, indicating that the micellar concentration is very low and that the interactions can be neglected. Therefore, the interparticle structure factor is reduced to unity; however, for the samples above this concentration, very broad interaction peaks appear in the intensity spectra. Moreover, as the concentration increases, the interaction peak increases in intensity, revealing an enhanced interparticle structure factor with increasing micellar concentration.

Furthermore, when the $I(Q)$ values at Q = 0.06–0.066 Å for the observed intensity spectra for oxy8, mxy8 and pxy8 were plotted against the inverse concen-

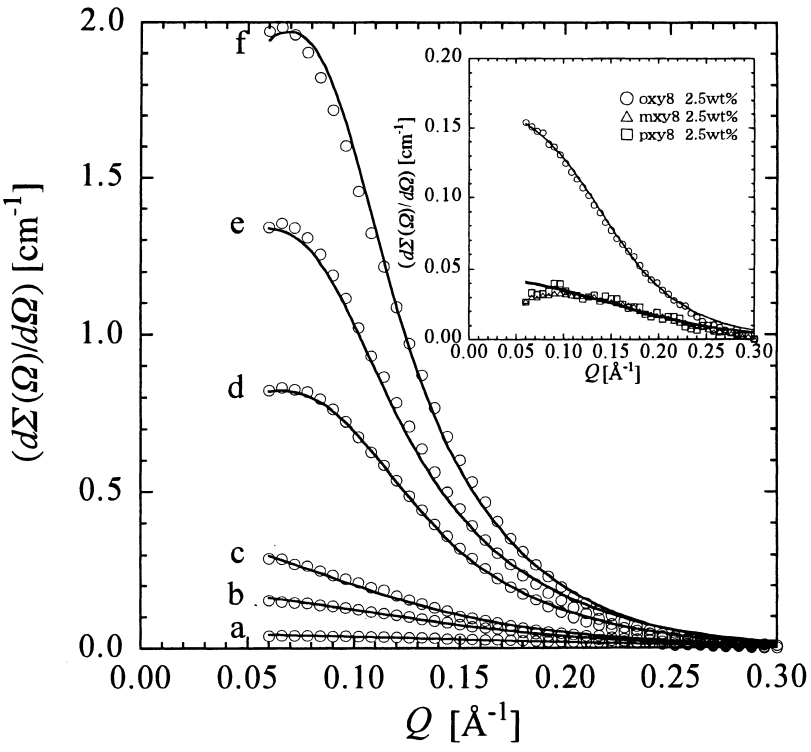

Fig. 3 Observed scattering intensity spectra (*open circles*) for the oxy8-D_2O system (*a*:2.0 wt%; *b*:2.5 wt%; *c*:3.0 wt%; *d*:4.0 wt%; *e*:5.0 wt%; *f*:6.0 wt%) at 23 °C and best-fit scattering intensity profiles (*solid lines*) (assuming monodispersity) and observed scattering intensity spectra (see *insert*) for mxy8-D_2O [2.5 wt%] (△) and pxy8-D_2O [2.5 wt%] (□) and best-fit scattering intensity profiles (*solid lines*). The *insert* also shows the observed spectrum for the oxy8-D_2O system (2.5 wt%) and its best-fit scattering intensity profile

tration, it was found that the plot provides two straight lines which intersect at 3.5 wt% (data not shown). This concentration is very close to the second cmc determined by conductivity and ^{1}H NMR chemical-shift methods and can be regarded as the second cmc of oxy8. Since the intensity spectra of oxy8, obtained below 3.5 wt%, as a whole, are very weak in intensity, we may expect that oxy8 micelles with a small aggregation number exist in this concentration region.

Thus, in this present study, for oxy8 sample solutions below the second cmc, analysis of the intensity spectra was carried out by assuming $S'(Q) = 1$. For the sample solutions above the second cmc, the RMSA procedure for calculation of $S'(Q)$ was used, and these $S'(Q)$ calculations used the more accurately prescribed diameter σ (Eq. 13–15).

The observed scattering intensity spectra were analyzed with the aggregation number (n), the degree of ionization of a micelle (α), and the number of hydrated methylene groups (n_{wet}) as fitting parameters. The values of a, b and t were calculated using n_{wet} and n. The values of the extracted parameters are listed in Table 3. The best-fit scattering intensity profiles for the oxy8 samples are also shown in Fig. 3. The closeness of fit between the observed and calculated data is excellent. The average percentage deviation per datum point was within ± 6% for all spectra.

Figure 4 shows the average aggregation number, n, plotted against $(X - X_{cmc})^{1/2}$, which is the square root of the monomer concentration (expressed as a molar fraction) attributable to formation of the oxy8 micelles. The plot provides two straight lines in the concentration range measured, indicating that the ladder model cannot be applied to micelles of geminis [35]. It should be noted that there is a marked difference in the slopes of the two straight lines below and above the second cmc, showing that marked growth in the oxy8 micelles occurs above the second cmc.

In the concentration region (2.0–3.0 wt%) between the first and second cmcs, the aggregation number (n) obtained for the oxy8 micelles is 3–7, indicating that the micellar size in this region is relatively small and that formation of premicelles rather than micelles may occur at the first cmc. Moreover, it is evident that micellar growth also occurs with an increase in concentration in this region, although the extent is small.

SANS analysis of small micelles has previously been made by Burkitt et al. [36] for micellar solutions of a simple surfactant (ammonium octanoate) in aqueous solution. The result showed that for these micelles the micellar shape is spherical and that the aggregation number depends upon the concentration ($n = 7$ at 0.36 mol l^{-1} and $n = 12$ at 0.48 mol l^{-1}). The aggregation numbers (n = 6–7) obtained below the second cmc for the gemini surfactant are very close to those for the micelles of ammonium octanoate in diluted solutions.

Extrapolation of the straight line of aggregation number, n versus $(X - X_{cmc})^{1/2}$ gives the minimum

Table 3 Fitted and derived parameters for oxy8 micellar solutions, assuming monodisperisty of micelles

wt%	n[a]	α[b]	n_{wet}[c]	a [Å][d]	b [Å][e]	t [Å][f]	$(a + t)/(b + t)$	N_S[g]	$1/\kappa$ [Å][h]	σ [Å][i]
2.0[j]	3.3	0.81	5.2	8.8	4.1	8.6	1.4	94		
2.5[j]	6.2	0.72	4.6	14.8	4.7	8.0	1.8	58		
3.0[j]	7.4	0.52	4.5	17.3	4.8	7.9	2.0	51		
4.0	19.6	0.16	3.4	25.2	7.3	8.3	2.1	32	10.8	42
5.0	28.2	0.16	3.4	36.2	7.3	8.3	2.8	27	10.6	49
6.0	36.8	0.16	1.4	40.1	9.8	5.8	2.9	16	8.5	49

[a] The aggregation number of a micelle
[b] The degree of ionization of a micelle
[c] The number of hydrated methylene groups in the Stern layer
[d] The major axis of a prolate micelle given by $a = (3V_{tail})/(4\pi nb^2)$
[e] The minor axis of a prolate micelle given by $b = \rho[1.5 + 1.265\ (8 - n_{wet})]$, where ρ is the ratio of a flexible to a fully extended chain ($\rho = 0.8$ for the 2.0–3.0 wt% sample and $\rho = 1$ for the 4.0–6.0 wt% samples)
[f] The thickness of the Stern layer given by equation $t = \rho[1.5 + 1.265\ (2 + n_{wet})]$
[g] The number of water molecules associated with a surfactant molecule
[h] The inverse Debye–Hückel screening length
[i] The macroion diameter, given by Eq. (12)
[j] The intensity spectra were calculated, assuming $S'(Q) = 1$ for these sample solutions

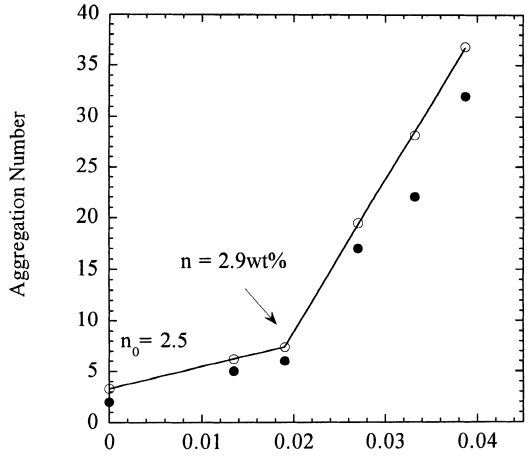

Fig. 4 Plot of the aggregation number, n, as a function of the square root of the monomer concentration (x = molar fraction) of assembling oxy8 micelles. The *open* (○) and *filled* (●) circles show the aggregation number calculated assuming monodispersity and polydispersity of the micelles, respectively

aggregation number (n) of a micelle at the cmc. The value of n_0 obtained for oxy8 is 3.3 (about 3), implying that the initial aggregation of the oxy8 ions at the first cmc involves formation of trimers as minimum submicelles, which then increase in size to form a range of small micelles with maximum aggregation number $n = 6$–7.

For sample solutions at concentrations greater than 3.0 wt%, the slope in the linear plots of n versus $(X - X_{cmc})^{1/2}$ tends to increase rapidly with an increase in concentration, showing that marked growth of the micelle occurs above this concentration. In addition to a rapid increase in aggregation number, the ratio of the axes, $(a + t)/(b + t)$, is found to increase rapidly at this concentration. The concentration 3.0 wt% is not in accord with the values (3.4 and 3.7 wt%) of the second cmc, which were determined by conductivity and ^{1}H NMR chemical-shift measurements, respectively; however, this concentration should be regarded as the second cmc obtained by using SANS analysis, since the value of the cmc depends upon the method used for its determination. Thus, we may assume that for oxy8 a marked variation in micellar size and shape occurs at the second cmc.

In this present study, the scattering intensity [$d\Sigma(Q)/d\Omega$] for oxy8 sample solutions was also calculated by considering the polydispersity (Eqs. 16, 17) and use was also made of the interparticle structure factor $S'(Q)$ for the samples above the second cmc [calculated $d\Sigma(Q)/d\Omega$ profiles are not shown]. The linear plots of n versus $(X - X_{cmc})^{1/2}$ are also shown in Fig. 4. It has been found that the calculated average aggregation number (n_{ave}) values are very close to the aggregation numbers calculated by assuming monodispersity. The calculated results are listed in Table 4.

We also used Eq. (5) to estimate the aggregation number of oxy8, mxy8 and pxy8. A Guinier plot of ln $d\Sigma(Q)/d\Omega$ against Q^2 is shown in Fig. 5. The radius of gyration (R_g), micellar weight and aggregation number are listed in Table 5. It is found that the aggregation numbers thus obtained are relatively close to those calculated by use of Eq. (3) [$S'(Q) = 1$ and $S'(Q) \neq 1$].

Both Vold [4] and Neuman and Gehlen [5] have previously presented the hypothesis (the gemini → submicelle → assembly model) that geminis might form submicellar aggregates such as dimers or tetramers in gemini solutions. Furthermore, Menger and Littau [2] provided ^{1}H and ^{23}Na NMR data for the xylene diphosphate geminis which supported this hypothesis.

Table 4 Fitted and derived parameter[a] for oxy8 micellar solutions, assuming polydispersity of micelles

wt%	n	α	n_{wet}	a [Å]	b [Å]	t [Å]	$(a + t)/(b + t)$	N_S	$1/\kappa$ [Å]	σ [Å]
2.0[b]	2	0.81	4.6	4.7	4.7	7.9	1.0	117		
2.5[b]	5	0.58	4.3	11.3	5.0	7.7	1.5	59		
3.0[b]	7	0.34	4.3	13.6	5.0	7.7	1.7	53		
4.0	17	0.17	3.5	22.2	7.2	8.5	2.0	34	10.8	40.7
5.0	22	0.11	3.5	28.7	7.2	8.5	2.3	30	10.8	44.5
6.0	32	0.11	3.3	40.6	7.4	8.2	3.1	24	10.7	51.0

[a] The definition of the parameters is given as footnotes to Table 3
[b] The intensity spectra were calculated assuming $S'(Q) = 1$ for these sample solutions

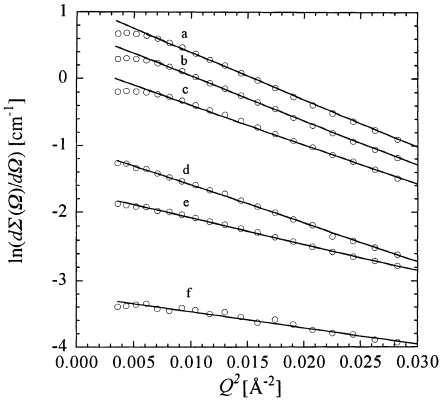

Fig. 5 The Guinier plots for the intensity spectra of oxy8 micellar solutions (*a*:2.0 wt%; *b*:2.5 wt%; *c*:3.0 wt%; *d*:4.0 wt%; *e*:5.0 wt%; *f*:6.0 wt%) at 23 °C

Table 5 Derived parameters for oxy8 micellar solutions, using a Guinier plot

Compound	R_g[a]	R [Å][b]	n[c]	Micellar weight
oxy8 2.0 wt%	8.6	11.0	7	3900
oxy8 2.5 wt%	10.7	13.9	13	7600
oxy8 3.0 wt%	13.0	16.8	23	13 000
oxy8 4.0 wt%	13.4	17.2	25	15 000
oxy8 5.0 wt%	14.1	18.3	30	17 000
oxy8 6.0 wt%	14.5	18.8	33	19 000
mxy8 2.5 wt%	6.6	8.5	3	1800
pxy8 2.5 wt%	7.1	9.1	4	2200

[a] Radius of gyration
[b] Apparent radius [Å] of a micelle
[c] Aggregation number

The SANS data of oxy8 micellar solutions may support the "gemini → submicelle → assembly" mechanism for the growing of oxy8 micelles. It may be assumed that micellization of gemini oxy8 proceeds as follows. Below the first cmc the gemini molecules are in the monomolecular dispersed state. At the first cmc, the oxy8 molecules mainly form trimers or tetramers as a minimum size premicelle. At low to intermediate concentrations (above the first cmc) secondary aggregation occurs between monomers and trimers (or tetramers or pentamers or hexamers) to form tetramers (or pentamers or hexamers or heptamers); that is, as the concentration further increases, secondary aggregation between premicelles of various sizes brings about formation of small micelles with small aggregation numbers, until the concentration reaches the second cmc. Above this concentration, further secondary aggregation between larger premicelles and small micelles or between the small micelles results in formation of larger micelles and simultaneously brings about variation in the micellar shape.

SANS spectra were also measured for D_2O solutions of mxy8 and pxy8 and the analysis of the scattering intensity spectra was also carried out using Eq. (3), [$S'(Q) = 1$]. The insert in Fig. 3 shows the SANS spectra of 2.5 wt% mxy8- and pxy8-D_2O solutions and the best-fit scattering intensity spectra. Compared with the intensity of the SANS spectrum oxy8, that for the scattering spectra of the two geminis (mxy8 and pxy8) is very small. This low intensity may be the result of the presence of the premicelles, including the dimers. Since the concentration of 2.5 wt% for the geminis of mxy8 and pxy8 is very close to the limits of their solubility at 23 °C and precipitation occurs at high concentrations, we could not measure the SANS spectra of more concentrated sample solutions. Therefore, we must assume that the mxy8 and pxy8 molecules may form only premicelles in water and that further aggregation to form micelles does not take place. In fact, the aggregation numbers (n) calculated for both the mxy8 and pxy8 solutions were about 2.

Such a difference in the solution behavior between the gemini oxy8 and the geminis mxy8 and pxy8 may be related to their molecular conformations, which are stabilized in the micellar state. For the conformation of an oxy8 molecule, which (as noted above) is stabilized in the micellar state, that N—^{s}C—^{a}C—^{a}C—^{s}C—N skeleton, including *o*-phenylenedimethylene, is planar. Furthermore, the conformation about the rigid ^{a}C—^{s}C single bond is gauche and the two *n*-octyl-N portions are in a trans configuration with respect to the ^{a}C—^{a}C double bond. Accordingly, when two *n*-octyl-N segments take up the all-trans form, it may be assumed that the two

n-octyl chains are not parallel to each other and fan out toward the methyl terminals of the *n*-octyl chains. Therefore, when the oxy8 molecules take up such a stabilized micellar structure, the packing feature of the *n*-octyl chains may be lost.

Conversely, for mxy8 molecules in their micellar state, the type I form (i.e., gg′gg′) is predominantly stabilized. In this conformation, the N—^{s}C—^{b}C—^{a}C—^{b}C—^{s}C—N skeleton takes up the all-trans form, leading to densely packed *n*-octyl chains within the micelles. This dense packing may result in a high-order (crystalline) self assembly. The molecular shape of the pxy8 molecule, probably favors formation of a densely packed state in concentrated solutions. This dense packing may then result directly in crystal formation from the premicellar state.

Micellar models

We are now in a position to discuss the model of a gemini micelle for oxy8, which takes into account the stacking pattern of the oxy8 molecules determined from our previous data for the ^{1}H chemical-shift variation of aromatic protons for oxy8, mxy8 and pxy8 upon micellization [37]. These data reflect the nature of the stacking about the aromatic rings of the nearest neighboring molecules, with the ^{1}H signals of the oxy8 aromatic protons being shifted downfield, while those of mxy8 and pxy8 aromatic protons are shifted upfield, showing that the aromatic protons of oxy8 are strongly influenced by the paramagnetic effect of a benzene-ring current and those of mxy8 and pxy8 by the diamagnetic effect of the ring current.

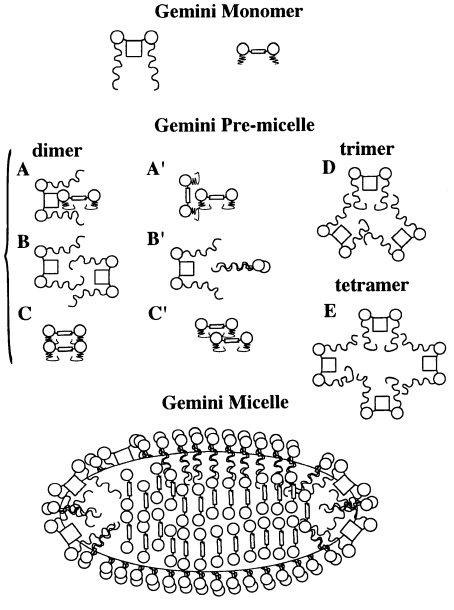

Fig. 6 Schematic model for the process of micellization

We may speculate six models, (A, A′ B, B′, C and C′) (Fig. 6), for the stacking feature of a oxy8 dimer. In models A, A′, B′, C and C′ the planar skeletons of the two oxy8 molecules are perpendicular to each other, leading to the up field shift of the aromatic protons signal, and in model B the two planar skeletons are parallel to each other and this stacking manner brings about the low-field shift of the aromatic ^{1}H signals.

Of the six models, we may select model B as the basis for a gemini premicelle or micelle. That is, the model which assembles dimers with monomers (or only dimers) brings about formation of premicelles with an aggregation numbers $n = 3$ or 4. By using this model, we can successfully account for the low-field shift of the aromatic protons of oxy8 upon micellization. However, as the micelle grows and its shape changes, the proportion of other types of stacking may increase.

The folded structure of *n*-octyl chains for oxy8 may play a significant role in a small micelle, since we may speculate that the CH_3CH_2 segment folded about $^{6}CH_2$—$^{7}CH_2$ bond fills the grooves among the oxy8 molecules.

For the micelles of oxy8 above the second cmc, the ratio of the axes, $(a+t)/(b+t)$, tends to increase markedly, showing that with increasing concentration, the micellar shape may become more cylindrical, rather than prolate. Such shape variation may bring about an increase of B-type stacking, since stacking of this type is favorable for the dense packing in the rod-like portion. For prolate or cylindrical micelles, in the portion with high curvature, the proportions of the fractions of other-type stacking (as well as those with B stacking), may increase. We may therefore emphasize that it is the variation of the stacking pattern at the second cmc which causes the marked variation in micellar shape.

For the stacking behavior of the premicelles of mxy8 and pxy8, we suggest model C or C′, in which the planar skeletons are stacked parallel to each other, as the basis for the premicelles, since, in these models, the aromatic protons may be influenced by the average diamagnetic effect of the benzene ring current and their ^{1}H signals will shift upfield upon premicellization.

References

1. Menger FM, Littau CA (1991) J Am Chem Soc 113:1451–1452
2. Menger FM, Littau CA (1993) J Am Chem Soc 115:10 083–10 090
3. Jiang X-K, Fan W-Q, Hui Y-Z (1984) J Am Chem Soc 106:7202–7205
4. Vold MJ (1990) J Colloid Interface Sci 135:520–530
5. Neumann MG, Gehlen MH (1990) J Colloid Interface Sci 135:209–217
6. Menger FM, Wood MG Jr, Richardson S, Zhou Q, Elrington AR, Sherrod MJ (1988) J Am Chem Soc 110: 6797–6803
7. Rice DK, Cadenhead DA, Lewis RNAH, McElhaney RN (1987) Biochemistry 26:3205–3210
8. Fahey D, Small DM (1988) Langmuir 4:589–594
9. Menger FM, Lee J-J, Aikens P, Davis S (1989) J Colloid Interface Sci 129: 185–191
10. Mann S, Schaffer TE, Huo Q, Hansma PK, Morse DE, Stucky GD, Aksay IA (1997) Langmuir 13:6382–6387
11. Song LD, Rosen MJ (1996) Langmuir 12:1149–1153
12. Hattori N, Yoshino A, Okabayashi H, O'Connor CJ (1998) J Phys Chem 102:8965–8973
13. Hattori N, Yoshino A, Okabayashi H (1996) In: Terao T (ed) Abstract (in Japanese) for the 35th Symposium on Nuclear Magnetic Resonance in Japan (Kyoto). 35th NMR Symposium office, pp 155–158
14. Zana R, Benrraou M, Rueff R (1991) Langmuir 7:1072–1075
15. (a) Vass S, Török T, Jákli G, Berecz E (1989) J Phys Chem 93:6553–6559; (b) Millero FJ, Surdo AL, Shin C (1978) J Phys Chem 82:784–792
16. Guinier A, Fournet G (1995) Small angle scattering of X-Rays. Wiley, New York
17. Lebowitz JL, Percus JK (1966) Phys Rev 144:251–258
18. Waisman E, Lebowitz JL (1972) J Chem Phys 56:3086–3093
19. Blum L, Hoye JS (1977) J Phys Chem 81:1311–1316
20. Triolo R, Floriano AM (1981) Adv Solution Chem 41–65
21. Hayter JB (1983) Faraday Discuss Chem Soc 76:7–17
22. Baus M, Hansen J-P (1980) Phys Rep 59:1–94
23. Palmer RG, Weeks JD (1973) J Chem Phys 58:4171–4174
24. Waisman E (1973) Mol Phys 25:45–48
25. Hayter JB, Penfold J (1981) Mol Phys 42:109–118
26. Hayter JB, Penfold J (1981) J Chem Soc Faraday Trans 1 77:1851–1863
27. Hansen J-P, Hayter JB (9182) Mol Phys 46:651–656
28. Kotlarchyk M, Chen SH (1983) J Chem Phys 79:2461–2469
29. Israelachvili JN (1992) Intermolecular and surface forces. Academic Press, London, pp 341–394
30. Okabayashi H, Okuyama M, Kitagawa T (1975) Bull Chem Soc Jpn 48:2264–2269
31. Okabayashi H, Taga K, Tsukamoto K, Tamaoki H, Yoshida T, Matsuura H (1985) Chem Scr 25:153–156
32. Schaufele RF, Shimanouchi T (1967) J Chem Phys 47:3605–3610
33. Hattori N, Yoshida H, Okabayashi H, O'Connor CJ, Zana R (1998) Vib Spectrosc 18:83–90
34. Tanford C (1974) J Phys Chem 78:2469–2479
35. Missel PJ, Mazer NA, Benedek GB, Young CY, Carey MC (1980) J Phys Chem 84:1044–1057
36. Burkitt SJ, Ottewill RH, Hayter JB, Ingram BT (1987) Colloid Polym Sci 256:619–627
37. Hattori N, Yoshino A, Okabayashi H (1997) In: Inagaki F (ed) Abstract (in Japanese) for the 36th Symposium on Nuclear Magnetic Resonance in Japan (Tokyo). 36th Symposium office, pp 217–220